Electromagnetic Loop Sensor

Chris Hynes* Rodney Vaughan

School of Engineering Science
Simon Fraser University
Burnaby, BC, Canada.

GASS 2020

SFU SIMON FRASER UNIVERSITY
ENGAGING THE WORLD

Outline

SFU SIMON FRASER UNIVERSITY ENGAGING THE WORLD

- Introduction and Background Theory
- Linearly Polarized Planewave Example
  - Theory
  - Simulation Results
- Dipole Moments Example
  - Theory
  - Simulation Results
- Conclusions

Introduction

- Electromagnetic (EM) field sensors have evolved from single port devices for measuring single field components, to few-port devices that measure multiple components, and finally multi-port devices for simultaneous measurement of all six field vector components.
  - These multi-port systems include antenna concepts for wireless mobile communications, often referred to as energy-density antennas.
  - Their basis is the combination of some or all of the EM field components - an idea attributed to John Robinson Pierce in the early 1960s[1].

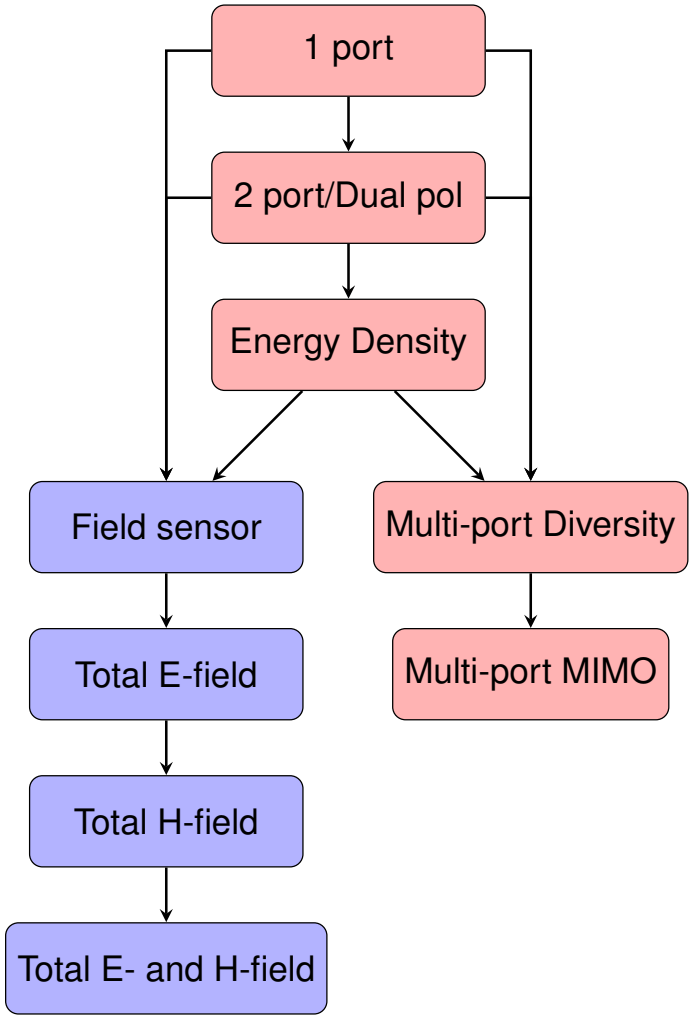

[1] R. Vaughan and J. Bach Andersen, *Channels, Propagation and Antennas for Mobile Communications*. Electromagnetic Waves Series 50, IEE, 2003

Dual-loaded Loop Sensor

- Using the loop Fourier analysis from the works of Storer[1] and Wu[2], Kanda[3] extended the analysis of Whiteside and King's dual-loaded loop sensor[4] for the case of general incident field distributions.
- In the present work, we rederive Kanda's results, proposing a small change which are validated with simulations.
- Throughout this paper complex notation is used and the time harmonic factor, $e^{j\omega t}$, has been suppressed.

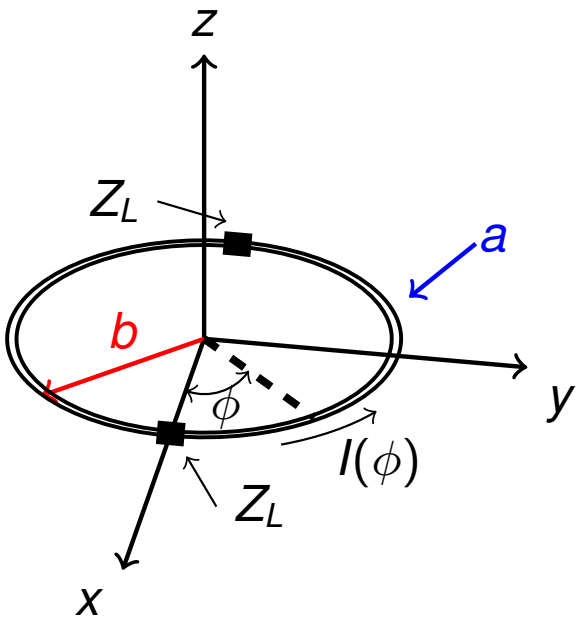

[1] (J. E. Storer, "Impedance of thin-wire loop antennas," *Transactions of the American Institute of Electrical Engineers, Part I: Communication and Electronics*, vol. 75, no. 5, pp. 606–619, 1956)

[2] (T. T. Wu, "Theory of the thin circular loop antenna," *Journal of Mathematical Physics*, vol. 3, no. 6, pp. 1301–1304, 1962)

[3] (M. Kanda, "An electromagnetic near-field sensor for simultaneous electric and magnetic-field measurements," *IEEE Transactions on Electromagnetic Compatibility*, vol. EMC-26, no. 3, pp. 102–110, Aug. 1984)

[4] (H. Whiteside and R.W.P. King, "The loop antenna as a probe," *IEEE Transactions on Antennas and Propagation*, vol. 12, no. 3, pp. 291–297, May 1964)

- The boundary conditions on a perfectly conducting loop with two antipodal loads are that the tangential electric field is zero everywhere except across the loads

$$-I(0)Z_L\delta(\phi) - I(\pi)Z_L\delta(\phi-\pi) = bE^i_\phi(b,\phi) + \frac{j\eta}{4\pi}\int_{-\pi}^{\pi} L(\phi-\phi')I(\phi')d\phi', \quad (1)$$

  where η is the wave impedance in the medium, Z_L the antipodal port impedances (assumed to be the same), $E^i_\phi(b,\phi)$ is the tangential component of the incident electric field on the loop surface, $L(\phi-\phi')$ is the integral kernel, and $I(\phi)$ loop current.

- The functions of ϕ are expressed as Fourier series

$$E^i_\phi(b,\phi) = \sum_{-\infty}^{\infty} f_n e^{-jn\phi} \quad \Rightarrow \quad f_n = \frac{1}{2\pi}\int_{-\pi}^{\pi} E^i_\phi(b,\phi)e^{jn\phi}d\phi, \quad (2)$$

$$I(\phi) = \sum_{-\infty}^{\infty} I_n e^{-jn\phi} \quad \Rightarrow \quad I_n = \frac{1}{2\pi}\int_{-\pi}^{\pi} I(\phi)e^{jn\phi}d\phi, \quad (3)$$

The integral kernel, $L(\phi - \phi')$, is also expressed as Fourier series

$$L(\phi) = \sum_{-\infty}^{\infty} a_n e^{-jn\phi}, \tag{4}$$

$$a_n = a_{-n} = \frac{kb}{2}\left(N_{n+1} + N_{n-1}\right) - \frac{n^2}{kb} N_n, \tag{5}$$

$$N_n = N_{-n} = \frac{1}{\pi} K_0\left(\frac{na}{b}\right) I_0\left(\frac{na}{b}\right) - \frac{1}{2}\int_0^{2kb} \left(\Omega_{2n}(x) + jJ_{2n}(x)\right) dx$$

$$+ \frac{1}{\pi}\left(\ln 4n + \gamma - 2\sum_{m=0}^{n-1} \frac{1}{2m+1}\right), \quad n \neq 0 \tag{6}$$

$$N_0 = \frac{1}{\pi} \ln \frac{8b}{a} - \frac{1}{2}\int_0^{2kb} \left(\Omega_0(x) + jJ_0(x)\right) dx. \tag{7}$$

Ω_n is the Lommel-Weber function, J_n is the Bessel function, $\gamma = 0.5772\cdots$ is Euler's constant, and I_0 and K_0 is the modified Bessel function of the first and second kind, respectively.

Substituting (2), (3) and (4) into (1) and performing the integration yields the Fourier series

$$-I(0)Z_L\delta(\phi) - I(\pi)Z_L\delta(\phi-\pi) = \sum_{-\infty}^{\infty}\left(\frac{j\eta}{2}a_n I_n + bf_n\right)e^{-jn\phi} \tag{8}$$

The coefficients for this Fourier series are

$$\frac{j\eta}{2}a_n I_n + bf_n = \frac{1}{2\pi}\int_{-\pi}^{\pi}\left(-I(0)Z_L\delta(\phi) - I(\pi)Z_L\delta(\phi-\pi)\right)e^{jn\phi}d\phi, \tag{9}$$

$$= -\frac{Z_L}{2\pi}\left(I(0) + I(\pi)e^{n\pi}\right), \tag{10}$$

from which the Fourier series coefficients for the loop current are

$$I_n = -\frac{2\pi bf_n}{j\pi\eta a_n} - \frac{Z_L}{j\pi\eta a_n}\left(I(0) + I(\pi)e^{n\pi}\right). \tag{11}$$

Theory

- For electrically small loops, the current can be approximated from the first few coefficients ($n < 2$) of its Fourier series.
- When this is done, using (3) and (11), the difference current between the ports is

$$I_\Delta = I(0) - I(\pi) = 2\left(I_1 + I_{-1}\right) = -\frac{2\pi b Y_1}{1 + 2Z_L Y_1}\left(f_1 + f_{-1}\right), \tag{12}$$

  where $Y_1 = 2/j\eta\pi a_1$ is the admittance of the $n = 1$ current mode. (12) is different from Kanda in that it doesn't assume that $f_1 = f_{-1}$ and that there is a sign change.
- The sum of the port currents is

$$I_\Sigma = I(0) + I(\pi) = 2I_0 = -\frac{4\pi b Y_0}{1 + 2Z_L Y_0} f_0, \tag{13}$$

  where $Y_0 = 1/j\eta\pi a_0$ is the admittance of the $n = 0$ current mode. (13) is different from Kanda in that there is a sign change.

Linearly Polarized Planewave

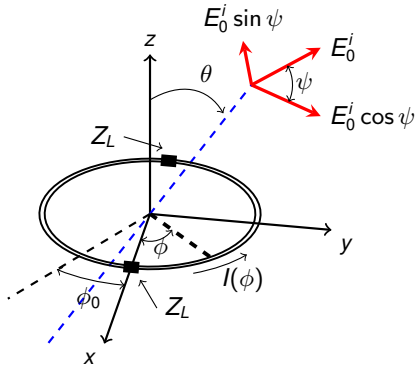

(a) Perspective view

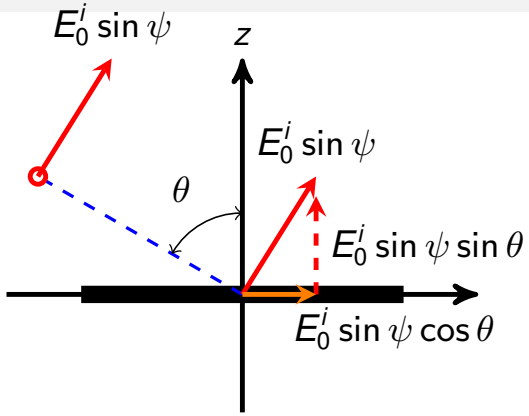

(b) Side (plane of incidence)

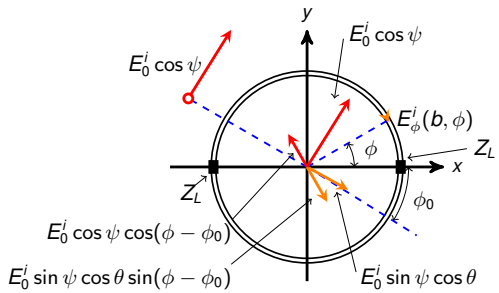

(c) Top view

For a linearly polarized planewave,

$$\boldsymbol{E}(r) = \boldsymbol{E}_0 e^{-j\boldsymbol{k}\cdot\boldsymbol{r}} = E_x\hat{\boldsymbol{x}} + E_y\hat{\boldsymbol{y}} + E_z\hat{\boldsymbol{z}} \tag{14}$$

$$= E_0^i\left(\left(-\cos\psi\sin\phi_0 + \sin\psi\cos\theta\cos\phi_0\right)\hat{\boldsymbol{x}} + \left(\cos\psi\cos\phi_0 + \sin\psi\cos\theta\sin\phi_0\right)\hat{\boldsymbol{y}} + \sin\psi\sin\theta\hat{\boldsymbol{z}}\right) \tag{15}$$

The magnetic intensity is

$$\boldsymbol{H}(r) = \frac{1}{\eta}\hat{\boldsymbol{k}} \times \boldsymbol{E} = H_x\hat{\boldsymbol{x}} + H_y\hat{\boldsymbol{y}} + H_z\hat{\boldsymbol{z}} = \frac{E_0^i e^{-j\boldsymbol{k}\cdot\boldsymbol{r}}}{\eta}\left(\left(\cos\psi\cos\theta\cos\phi_0 + \sin\psi\sin\phi_0\right)\hat{\boldsymbol{x}} + \left(\cos\psi\sin\phi_0\cos\theta - \sin\psi\cos\phi_0\right)\hat{\boldsymbol{y}} + \cos\psi\sin\theta\hat{\boldsymbol{z}}\right). \tag{16}$$

E_ϕ Fourier coefficients for planewave

The ϕ-component of the electric intensity (15) along a $\hat{\boldsymbol{z}}$-directed loop of radius b, located at the origin, is

$$E^i_\phi(b,\phi) = E^i_0\left(\cos\psi\cos\left(\phi-\phi_0\right) - \sin\psi\sin\left(\phi-\phi_0\right)\cos\theta\right) e^{jkb\cos(\phi-\phi_0)\sin\theta} \tag{17}$$

$$= \sum_{-\infty}^{\infty} f_n e^{-jn\phi} \tag{18}$$

where

$$f_n = \frac{1}{2\pi}\int_{-\pi}^{\pi} E^i_\phi(b,\phi) e^{jn\phi}\, d\phi \tag{19}$$

$$= -j^{-n} e^{jn\phi_0}\left(\sin\psi\cos\theta\frac{nJ_n\left(kb\sin\theta\right)}{kb\sin\theta} + j\cos\psi J'_n(kb\sin\theta)\right) \tag{20}$$

Current response for planewave

From (20),

$$f_0 = j\cos\psi J_1(kb\sin\theta) \tag{21}$$

$$\approx -j\frac{kb}{2}\cos\psi\sin\theta \tag{22}$$

$$f_1 + f_{-1} = 2\cos\phi_0\cos\psi J_1'(kb\sin\theta) - 2\sin\phi_0\sin\psi\cos\theta\frac{J_1(kb\sin\theta)}{kb\sin\theta} \tag{23}$$

$$\approx \cos\phi_0\cos\psi + \sin\phi_0\sin\psi\cos\theta \tag{24}$$

Comparing (22) and (24) to the field expressions for the electric and magnetic intensities (15) and (16), yields

$$I_\Sigma = I(0) + I(\pi) = \frac{j2\pi kb^2\eta Y_0}{1 + 2Y_0Z_L}H_z \tag{25}$$

$$I_\Delta = I(0) - I(\pi) = -\frac{2\pi bY_1}{1 + 2Y_1Z_L}E_y \tag{26}$$

Simulation Results

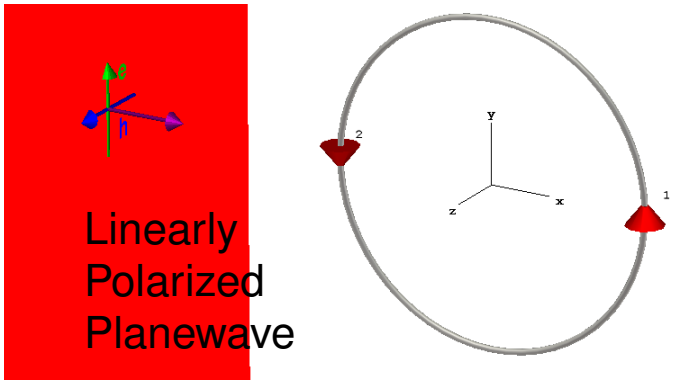

(d) Simulation model

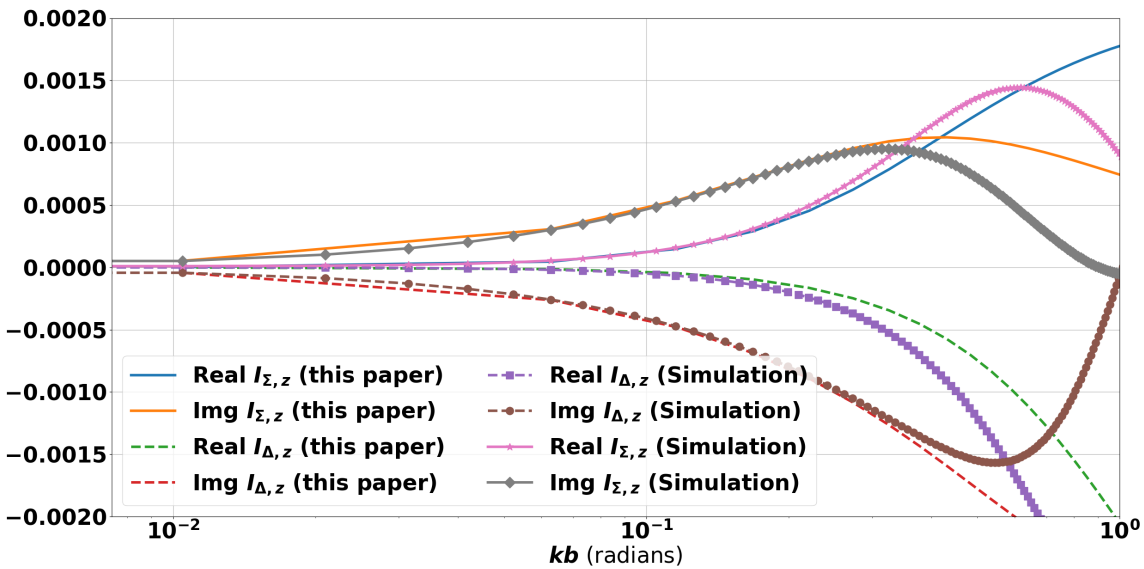

(e) Results using (25) and (26)

Figure: (a) Plane wave propagating in the $+\hat{\boldsymbol{x}}$-direction, polarized in the $+\hat{\boldsymbol{y}}$-direction (i.e. $\psi = 0$, $\theta = \pi/2$, and $\phi_0 = 0$). (b) (25) compared against (26) and show excellent agreement when $kb < 0.2$ ($Z_L = 315$).

Centrally located dipole moments

- Kanda and Hill extended the application of a dual-loaded loop to detecting centrally located electric and magnetic dipole moments[1]
- The azimuthal electric field is

$$E_\phi^i = m_{m,z} G_m + m_{e,y} G_e \cos\phi - m_{e,x} G_e \sin\phi, \tag{27}$$

where,

$$G_m = \frac{\eta}{4\pi}\left(\frac{k^2}{b} - \frac{jk}{b^2}\right) e^{-jkb}, \tag{28}$$

$$G_e = -\frac{\eta}{4\pi}\left(\frac{jk}{b} + \frac{1}{b^2} + \frac{1}{jkb^3}\right) e^{-jkb}. \tag{29}$$

and m_{ej} and m_{mj} are the Cartesian components of the centrally located electric and magnetic dipole moment.

[1] M. Kanda and D. A. Hill, "A three-loop method for determining the radiation characteristics of an electrically small source," *IEEE Transactions on Electromagnetic Compatibility*, vol. 34, no. 1, pp. 1–3, Feb. 1992.

Current response from dipole moments

The Fourier series coefficients for (27) are

$$f_0 = m_{m,z} G_m, \tag{30}$$

$$f_1 = \frac{m_{e,y} G_e}{2} + \frac{m_{e,x} G_e}{2j}, \tag{31}$$

$$f_{-1} = \frac{m_{e,y} G_e}{2} - \frac{m_{e,x} G_e}{2j}, \tag{32}$$

$$f_1 + f_{-1} = m_{e,y} G_e. \tag{33}$$

The sum and difference currents to components of the moments,

$$I_\Sigma = I(0) + I(\pi) = -\frac{4\pi b Y_0 G_m}{1 + 2 Y_0 Z_L} m_{m,z}, \tag{34}$$

$$I_\Delta = I(0) - I(\pi) = -\frac{2\pi b Y_1 G_e}{1 + 2 Y_1 Z_L} m_{e,y}. \tag{35}$$

Note that (35) is half of the value presented in previous work[1,2], and both (34) and (35) differ from the previous work by a sign change.

[1] M. Kanda and D. A. Hill, "A three-loop method for determining the radiation characteristics of an electrically small source," *IEEE Transactions on Electromagnetic Compatibility*, vol. 34, no. 1, pp. 1–3, Feb. 1992.

[2] S. Tofani, P. Ossola, G. d'Amore, *et al.*, "A three-loop antenna system for performing near-field measurements of electric and magnetic fields from video display terminals," *IEEE Transactions on Electromagnetic Compatibility*, vol. 38, no. 3, pp. 341–347, Aug. 1996.

Simulation of magnetic moment

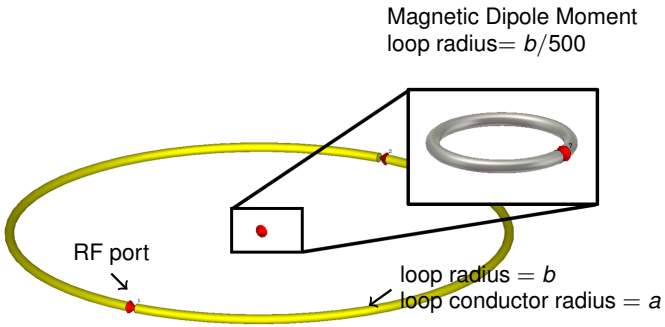

(a) Simulation model.

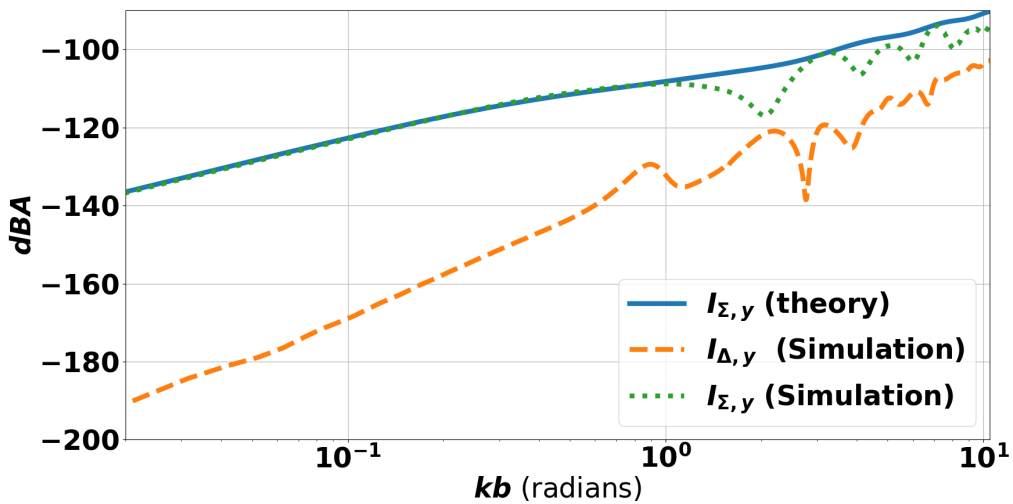

(b) Simulation results ($I = 1A$).

Figure: $\hat{y}$-directed loop with a $\hat{y}$-directed magnetic dipole source at the centre. $a = b/52$, the port gaps $= 2a$, and the magnetic dipole radius $= b/500$.

Simulation of electric moment

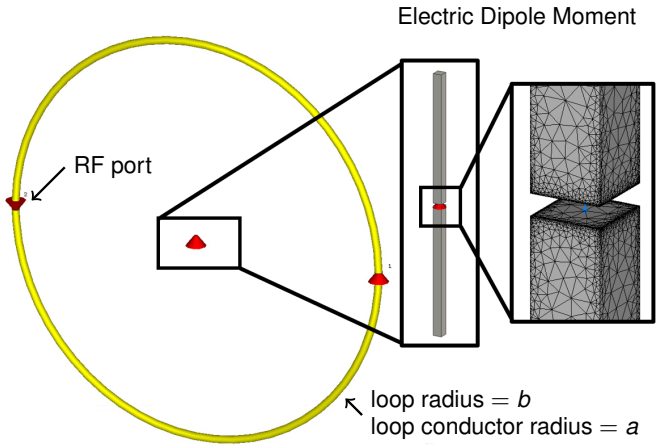

(a) Simulation model.

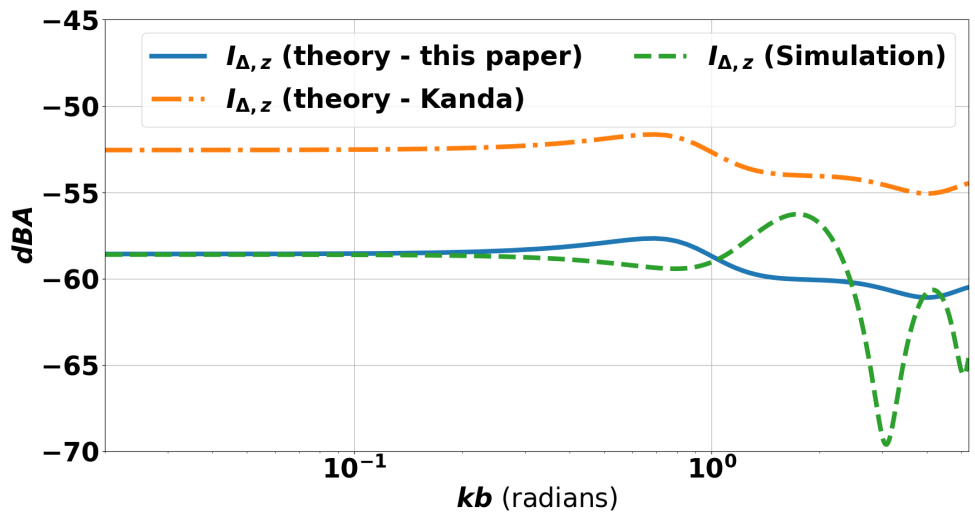

(b) Simulation results.

Figure: Centrally located electric dipole source. ($a = b/52$, port gaps $= 2a$, dipole length $= b/83$, dipole width $= b/7,500$, and the dipole feed gap $= b/25,000$)

Conclusions

- Presented the theory of coupling incident electric field onto an electrically small dual-loaded loop.
  - Propose a small correction to the pre-existing theory.
- Performed simulations to compare simulation results to theory
  - Linearly polarized planewaves agree well with theory (sign change)
  - The coupling from the magnetic dipole moment was straight forward to simulate and agreed with theory.
  - The coupling from the electric dipole moment was challenging to simulate and the results agree with the small proposed corrections to the theory.

Acknowledgement

We acknowledge the financial support of the Natural Sciences and Engineering Research Council of Canada (NSERC), [funding reference number CGSD2-535282-2019].

Cette recherche a été financée par le Conseil de recherches en sciences naturelles et en génie du Canada (CRSNG), [numéro de référence CGSD2-535282-2019].

Further questions can be sent to:

Chris Hynes - c_h@sfu.ca
Rodney Vaughan - rodney_vaughan@sfu.ca